RESEARCH ARTICLE

Figures and figure supplements

Phosphoproteomic mapping reveals distinct signaling actions and activation of muscle protein synthesis by Isthmin-1

Meng Zhao *et al*

Figure 1. Phosphoproteomics reveals overlapping and distinct pathways of Ism1 and insulin. (**A**) Experimental design of the untargeted phosphoproteomics analysis. 3T3-F442A cells were serum-starved for 16 hr and treated with 100 nM recombinant Ism1 or insulin for 5 min (n = 6 biological replicates per group were pooled and then divided into n = 2 technical replicates). Proteins were extracted, trypsin digested, and fractionated. Phosphopeptides were enriched using TiO_2 chromatography, and phosphopeptides were analyzed with LC-MS/MS. (**B**) Western blot

Figure 1 continued on next page

Figure 1 continued

analysis of p-AKT^{S473}, total AKT, and β-actin in cells treated with 100 nM bovine serum albumin (BSA), 100 nM Ism1, or 100 nM insulin for 5 min (Western blot n = 2 pooled from n = 6 per treatment group; quantification n = 4 combining three independent assays). p-Values are calculated by one-way ANOVA, *p<0.05, **p<0.01, ****P*p0.001. (**C**) Protein intensity-based principal component analysis (PCA) of the phosphoproteomic dataset. (**D**) Venn diagram of the phosphopeptides detected in both replicates after BSA-, Ism1-, or insulin treatment. (**E**) Heatmap of differentially phosphorylated peptides with 100 lowest significant p-values (adj. p<0.05) from three comparisons displayed as log2 ratio (BSA vs. Ism1, BSA vs. insulin, and insulin vs. Ism1). (**F**) Distribution diagram of shared and unique phosphosites (detected in at least one sample) between treatments for selected Gene Ontology (GO) pathways. Inner links in shades show phosphosites detected in two or more treatment conditions. Gray shows phosphosites detected in all samples; purple shows phosphosites detected in both Ism1 and insulin-treated cells; green shows phosphosites detected in both BSA and insulin-treated cells; blue shows phosphosites detected in both BSA- and Ism1-treated cells. The middle ring displays GO pathway/pathway group with ticks indicating the number of phosphopeptides. Large ticks indicate 50 phosphopeptides, and small ticks indicate 5 phosphopeptides. The outer ring displays gene symbols and the phosphosite exclusively detected in each treatment. See also ***Figure 1—figure supplement 1*** and ***Figure 1—source data 1***, ***Figure 1—source data 2***, and ***Figure 1—source data 3***.

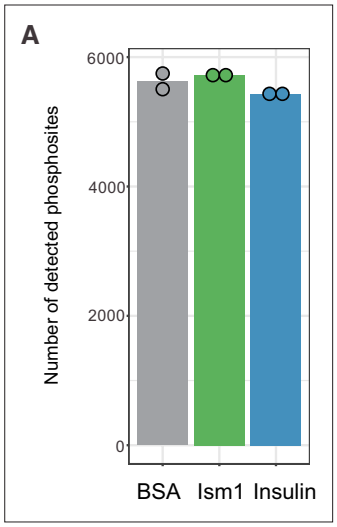

Figure 1—figure supplement 1. Quality controls for the phosphoproteomics analysis.

Figure 2. Phospho-specific mapping identifies an Ism1-induced signature consistent with protein translation and muscle function. (**A**) Venn diagram of shared and unique phosphosites between treatments for the Gene Ontology (GO) pathways Insulin. (**B**) Abundance of InsR Y1175/1163 in cells treated with bovine serum albumin (BSA), Ism1, or insulin (n = 2). Individual comparisons between conditions across phosphopeptides were performed using empirical Bayes statistics followed by adjustment for multiple testing using false discovery rate, *p<0.05, **p<0.01, ***p<0.001. The minimum

Figure 2 continued on next page

Figure 2 continued

normalized intensity across the dataset was subtracted from each normalized data point, and phosphorylation was calculated as a fraction of the maximum value of all samples for each phosphopeptide. Bars show mean ± SEM. (**C**) Venn diagram of shared and unique phosphosites between treatments for the GO pathways Insulin mTOR. (**D**) Venn diagram of shared and unique phosphosites between treatments for the GO pathways and muscle. (**E–N**) Abundance of proteins with indicated phosphosite in cells treated with BSA, Ism1, or insulin (n = 2). Individual comparisons between conditions across phosphopeptides were performed using empirical Bayes statistics followed by adjustment for multiple testing using false discovery rate, *p<0.05, **p<0.01, ***p<0.001. The minimum normalized intensity across the dataset was subtracted from each normalized data point, and phosphorylation was calculated as a fraction of the maximum value of all samples for each phosphopeptide. Note that, in case of non-detectable phosphopeptides, significance testing was based on imputed values, n.d., non-detectable. Bars show mean ± SEM. (**O**) Ism1 signaling network in 3T3-F442A cells. Ism1 ligand stimulation triggers activation of the PI3K/AKT pathway and the mTORC1 pathway, which leads to changes in phosphorylation status of multiple proteins involved in protein translation and muscle function. (**P**) Pathway analysis of enriched GO pathways in the Ism1 group versus BSA. Clusters are dominated by (1) mixed terms, (2) metabolic process, (3) development, and (4) localization/transport. Plotted GO terms all have p-values <0.01 calculated using the classic Kolmogorov–Smirnov test. See also ***Figure 2—figure supplement 1***, ***Figure 2—source data 1***, and ***Figure 2—source data 2***.

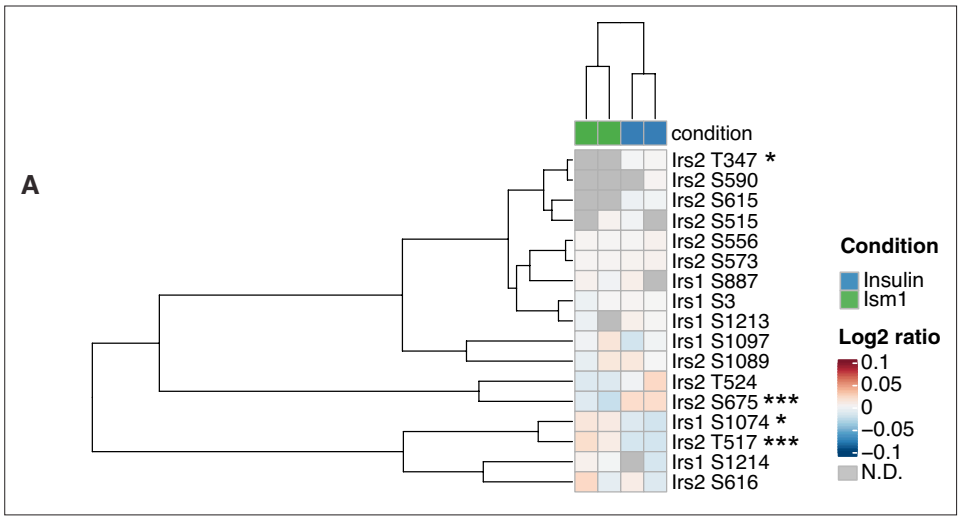

Figure 2—figure supplement 1. Insulin receptor substrate-1 and 2 (Irs1/2) phosphorylation status in response to Ism1 or insulin. (**A**) Heatmap of differentially phosphorylated Irs1 and Irs2 phosphosites by Ism1 relative to insulin (n = 2, individual comparisons between conditions across phosphopeptides using empirical Bayes statistics followed by adjustment for multiple testing using false discovery rate, *p<0.05, **p<0.01, ***p<0.001).

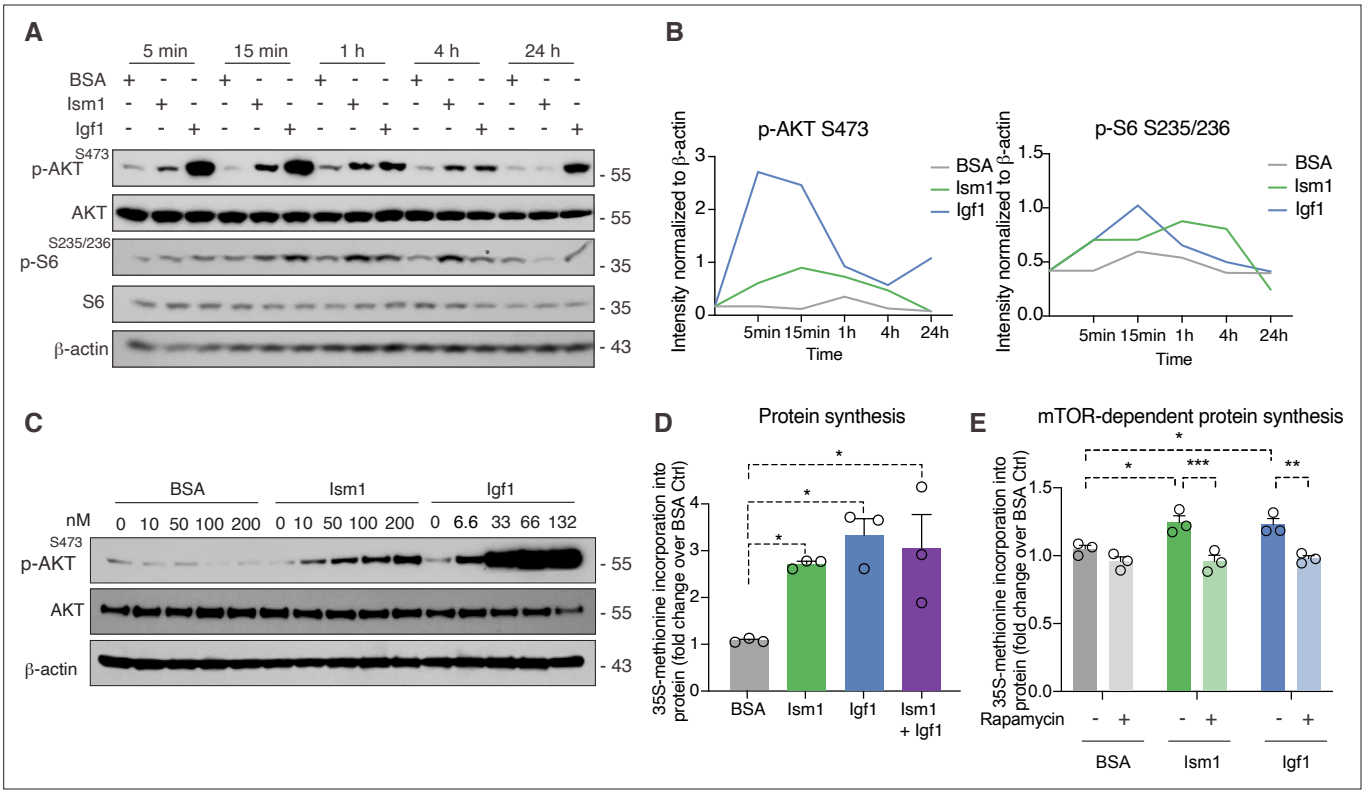

Figure 3. Ism1 induces mTOR-dependent protein synthesis in muscle cells. (**A**) Western blot analysis of p-AKT^{S473}, total AKT, p-S6$^{S235/}$236, total S6, and β-actin in C2C12 myotubes treated with 100 nM bovine serum albumin (BSA), 100 nM Ism1, or 50 ng/ml Igf1. (**B**) Quantification of protein expression of p-AKT S473/β-actin and p-S6 S235/236/β-actin. (**C**) Western blot analysis of p-AKT^{S473}, total AKT, and β-actin in C2C12 myoblasts treated with indicated concentrations of BSA, Ism1, or Igf1 for 5 min. (**D**) Levels of protein synthesis measured by [^{35}S]-methionine incorporation in C2C12 myotubes after 48 hr of indicated treatments (n = 3, one-way ANOVA, *p<0.05, **p<0.01, ***p<0.001). (**E**) Levels of protein synthesis measured by [^{35}S]-methionine incorporation in C2C12 myotubes with indicated treatments for 2 hr in the presence or absence of 100 nM of the mTOR inhibitor rapamycin (n = 3, two-way ANOVA, *p<0.05, **p<0.01, ***p<0.001). Bar graphs show mean ± SEM. See also ***Figure 3—source data 1*** and ***Figure 3—source data 2***.

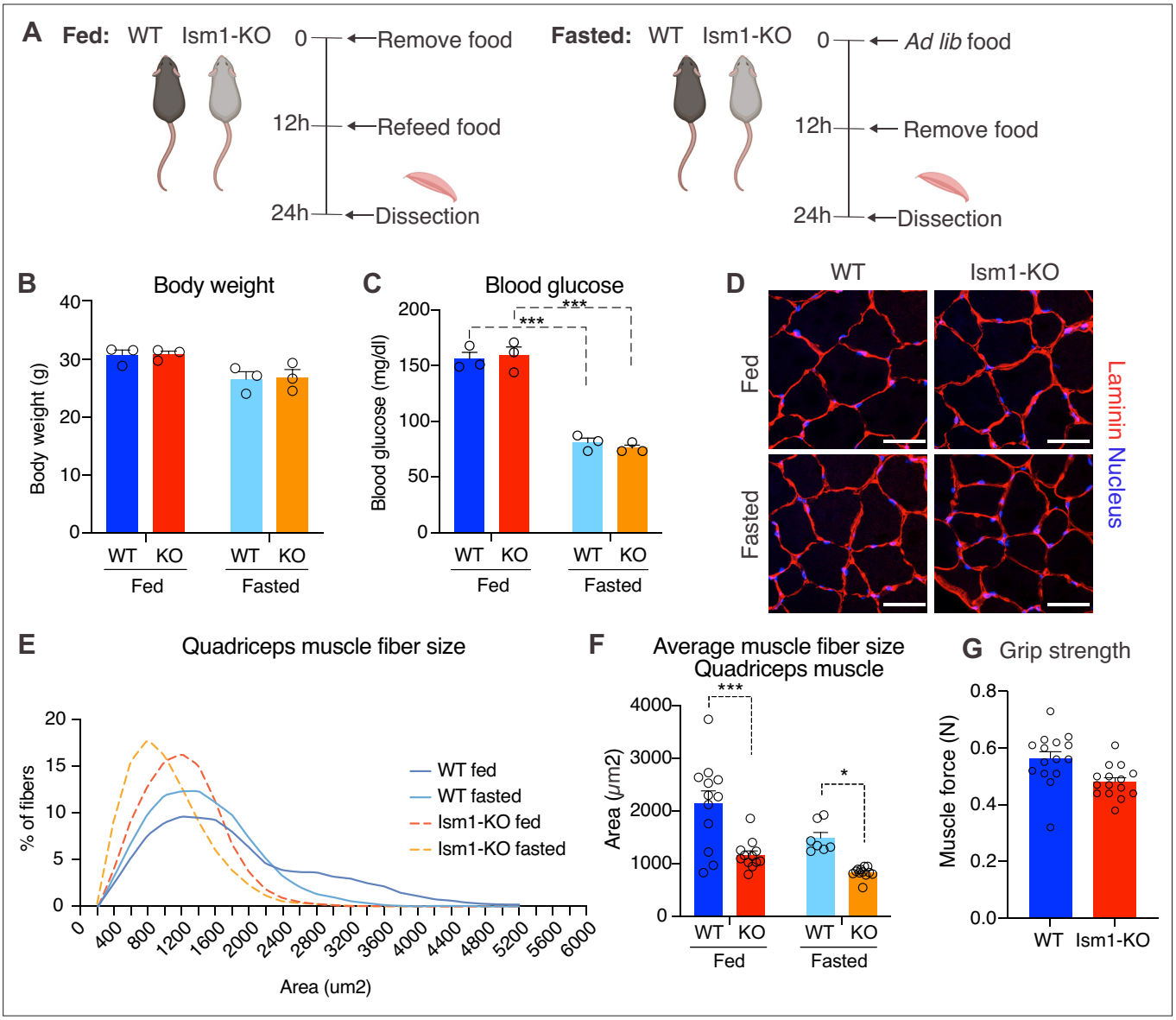

Figure 4. *Ism1* ablation results in reduced skeletal muscle fiber size and muscle strength. (**A**) Schematic description of the fasting and feeding protocol. (**B**) Body weights of WT and *Ism1*-KO mice in the fed or fasted groups (WT fed, n = 3; *Ism1*-KO fed, n = 3; WT fasted, n = 3; *Ism1*-KO fasted, n = 3, two-way ANOVA). (**C**) Blood glucose level in fed and fasted mice before dissection (WT fed, n = 3; *Ism1*-KO fed, n = 3; WT fasted, n = 3; *Ism1*-KO fasted, n = 3, two-way ANOVA, *p<0.05, **p<0.01, ***p<0.001). (**D**) Immunolabeling of laminin (red), staining of nucleus (blue) of mouse quadriceps muscles from WT and *Ism1*-KO mice in the fed or fasted groups (scale bars: 10 μm). Images are representative examples of three mice showing similar results. (**E**) Fiber size distribution of mouse quad muscles (WT fed, n = 3; *Ism1*-KO fed, n = 3; WT fasted, n = 3; *Ism1*-KO fasted, n = 3). Mean percentage of myofibers within the indicated range is shown. (**F**) Quantification of average muscle fiber area (WT fed, n = 3; *Ism1*-KO fed, n = 3; WT fasted, n = 3; *Ism1*-KO fasted, n = 3, one muscle tissue per mouse, 2–4 images per muscle tissue,~60–100 myofibers quantified per image; two-way ANOVA, *p<0.05, **p<0.01, ***p<0.001) performed in a blinded fashion by two independent investigators. This experiment was repeated using two independent cohorts of mice. (**G**) Grip strength measured by two-paw muscle force (**N**) on a grid in WT and *Ism1*-KO mice (WT, n = 15; *Ism1*-KO, n = 15). p-Values are calculated by two-tailed Student's *t*-test, *p<0.05, **p<0.01, ***p<0.001. Bar graphs show mean ± SEM. See also ***Figure 4—figure supplements 1 and 2*** and ***Figure 4—source data 1***.

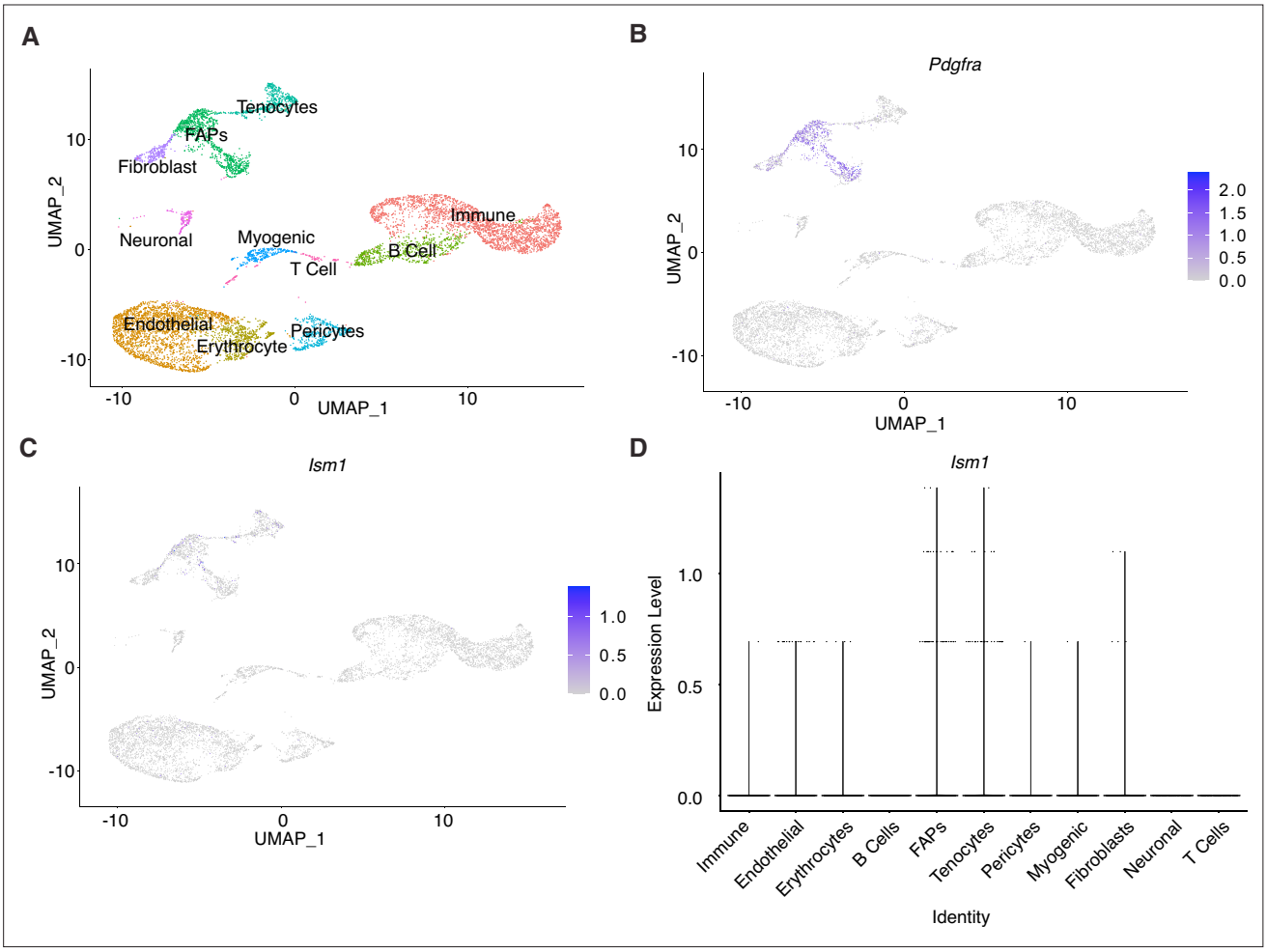

Figure 4—figure supplement 1. Ism1 acts non-cell-autonomously on muscle cells. (**A**) UMAP plot of single-cell RNA sequencing of isolated cells from mouse skeletal muscle. (**B**) Expression of *Pdgfra* in fibro-adipose precursors within the muscle. (**C**) Low expression of *Ism1* within the muscle tissue. (**D**) Low expression of *Ism1* in myocytes and myoblasts.

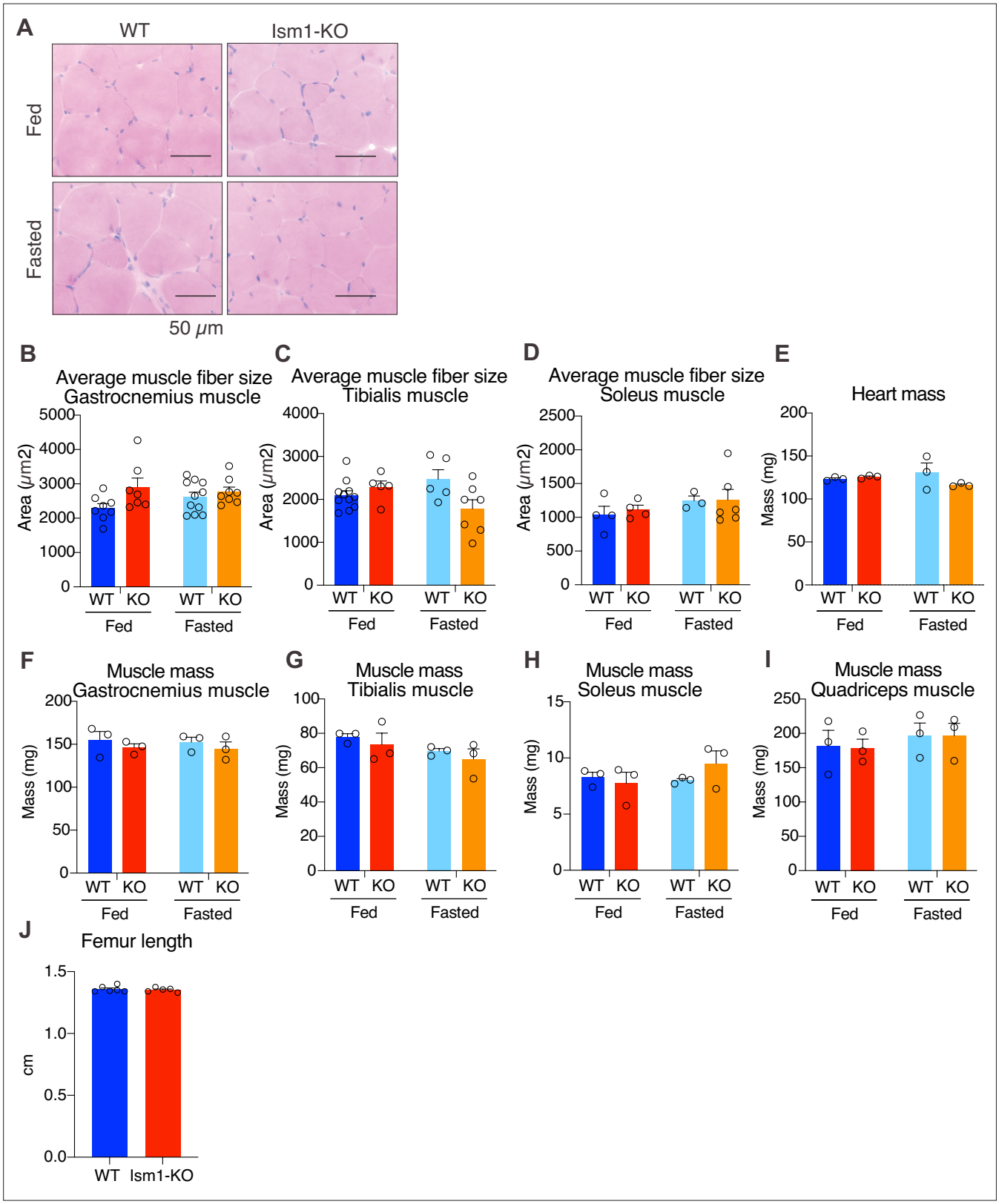

Figure 4—figure supplement 2. *Ism1* ablation does not reduce muscle mass or muscle fiber size in all tissue locations. (**A**) Hematoxylin and eosin (H&E) staining of mouse quadriceps muscles from WT and *Ism1*-KO mice in the fed or fasted groups (scale bars: 50 μm). Images are representative examples of three mice showing similar results. (**B–D**) Quantification of average muscle fiber area in gastrocnemius (**B**) tibialis (**C**), and soleus (**D**) in a blinded fashion by two independent investigators (WT fed, n = 3; *Ism1*-KO fed, n = 3, WT fasted, n = 3; *Ism1*-KO fasted, n = 3, two-way ANOVA,

Figure 4—figure supplement 2 continued on next page

Figure 4—figure supplement 2 continued

*p<0.05, **p<0.01, ***p<0.001). (**E**) Heart mass of WT and *Ism1*-KO mice in the fed or fasted groups (WT fed, n = 3; *Ism1*-KO fed, n = 3; WT fasted, n = 3; *Ism1*-KO fasted, n = 3, two-way ANOVA). (**F–H**) Muscle masses of gastrocnemius (**F**), tibialis (**G**), soleus (**H**), and quadriceps (**I**) of WT and *Ism1*-KO mice in the fed or fasted groups (WT fed, n = 3; *Ism1*-KO fed, n = 3; WT fasted, n = 3; *Ism1*-KO fasted, n = 3, two-way ANOVA). (**J**) Femur length measured in WT and *Ism1*-KO (WT, n = 6; *Ism1*-KO, n = 5, two-tailed Student's *t*-test *p<0.05, **p<0.01, ***p<0.001). Bar graphs show mean ± SEM.

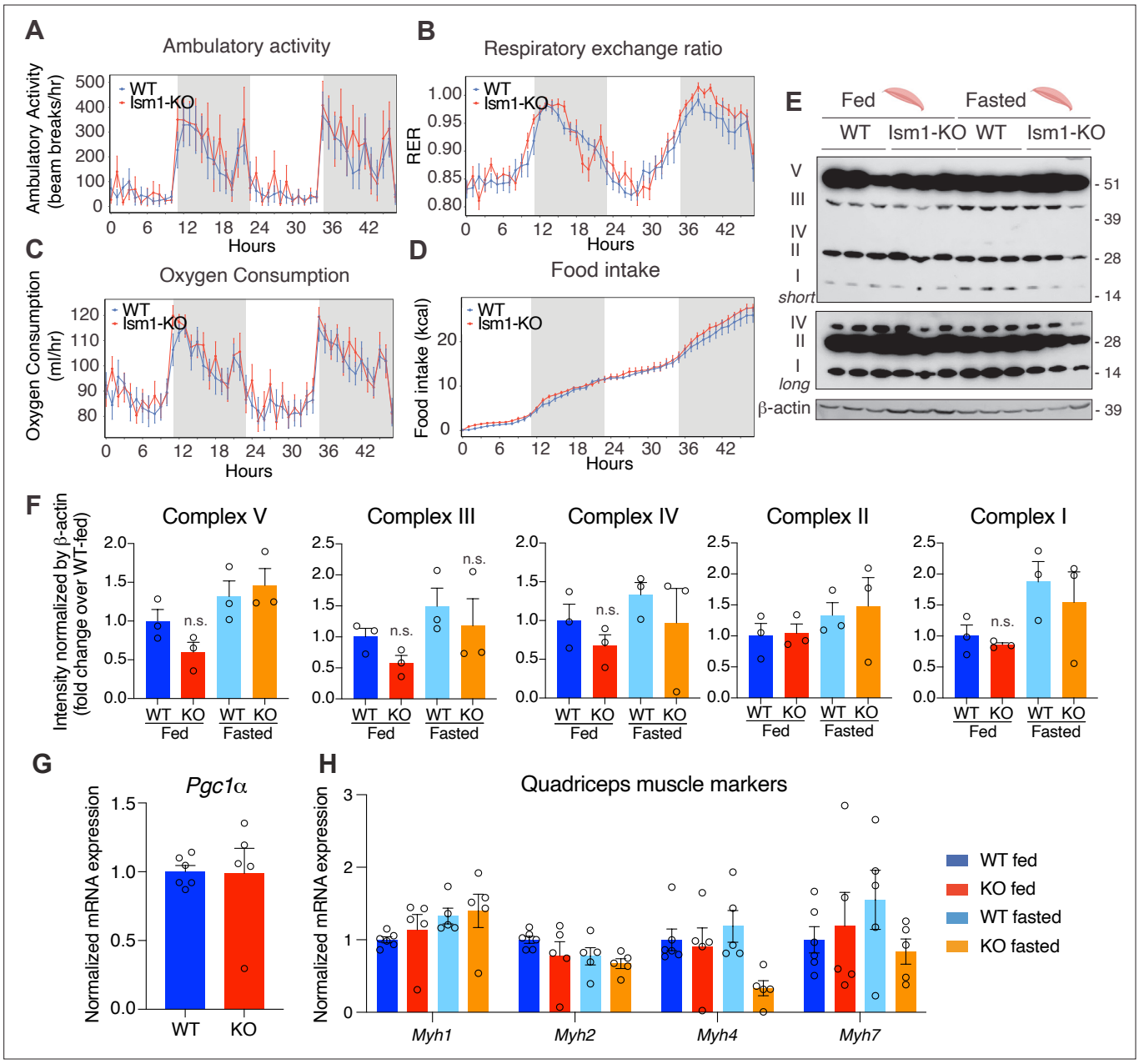

Figure 5. *Ism1* ablation does not impair movement, mitochondrial biogenesis, or normal muscle development. (**A**) Ambulatory activity (WT, n = 4; *Ism1*-KO, n = 4, ANOVA, *p<0.05). (**B**) Respiratory exchange ratio (RER) (WT, n = 4; *Ism1*-KO, n = 4, ANOVA, *p<0.05). (**C**) Oxygen consumption (WT, n = 4; *Ism1*-KO, n = 4, ANCOVA, *p<0.05). (**D**) Food intake (WT, n = 4; *Ism1*-KO, n = 4, ANCOVA, *p<0.05) in WT and Ism1-KO mice. Mice were habituated for 24 hr followed by 48 hr recordings of metabolic parameters. (**E**) Levels of mitochondrial oxidative phosphorylation proteins in ETC complexes (OXPHOS) from quadriceps muscles (WT fed, n = 3; *Ism1*-KO fed, n = 3; WT fasted, n = 3; *Ism1*-KO fasted, n = 3) analyzed by Western blot. (**F**) Quantification of OXPHOS complexes (two-way ANOVA, *p<0.05, **p<0.01, ***p<0.001). (**G**) Relative gene expression analysis of *Pgc1α* in quadriceps muscle from WT (n = 6) or *Ism1*-KO (n = 5) mice (two-tailed Student's *t*-test, *p<0.05, **p<0.01, ***p<0.001). (**H**) Relative gene expression analysis of *Myh1, Myh2, Myh4*, and *Myh7* in quadriceps muscle from WT fed (n = 6) or *Ism1*-KO fed (n = 5) vs. WT fasted (n = 5) or *Ism1*-KO fasted (n = 5) mice (two-way ANOVA, *p<0.05, **p<0.01, ***p<0.001). Bar graphs show mean ± SEM. See also ***Figure 5—source data 1*** and ***Figure 5—source data 2***.

Figure 6. *Ism1*-KO mice have defective skeletal muscle protein synthesis and AKT-mTOR signaling. (**A**) Total protein content measured in WT and *Ism1*-KO quadriceps muscle expressed as mg protein/wet tissue weight in grams. (WT, n = 12; *Ism1*-KO, n = 9, two-tailed Student's *t*-test, *p<0.05, **p<0.01, ***p<0.001). (**B**) Schematic description of the in vivo [^{35}S]-methionine incorporation protocol. (**C**) In vivo protein synthesis measured by [^{35}S]-methionine incorporation in WT and *Ism1*-KO mice (WT, n = 12; *Ism1*-KO, n = 9, two-tailed Student's *t*-test, *p<0.05, **p<0.01, ***p<0.001). Relative gene

Figure 6 continued on next page

Figure 6 continued

expression analysis of (**D**) *FoxO* and (**E**) *FoxO* target genes *Cdkn1b, Eif4ebp1,* and *Ctsl* in quadriceps muscle from WT fed (n = 6) or *Ism1*-KO fed (n = 5) vs. WT fasted (n = 5) or *Ism1*-KO fasted (n = 5) mice (two-way ANOVA, *p<0.05, **p<0.01, ***p<0.001). (**F**) Western blot analysis and quantification of the levels of p27 and tubulin in the cytosolic fraction of quadriceps muscles of WT and *Ism1*-KO mice under fed and fasted conditions (WT fed, n = 3; *Ism1*-KO fed, n = 3, WT fasted, n = 3; *Ism1*-KO fasted, n = 3, two-way ANOVA, *p<0.05, **p<0.01, ***p<0.001). (**G**) Western blot analysis and quantification of the levels of pAKT^{S473}, total AKT, p-mTOR^{S2448}, total mTOR, pS6$^{S235/236}$, total S6, and β-actin in quadriceps muscles of WT and *Ism1*-KO mice under fed and fasted conditions (WT fed, n = 3; *Ism1*-KO fed, n = 3, WT fasted, n = 3; *Ism1*-KO fasted, n = 3, two-way ANOVA, *p<0.05, **p<0.01, ***p<0.001). Bar graphs show mean ± SEM. See also ***Figure 6—figure supplement 1***, ***Figure 6—source data 1***, and ***Figure 6—source data 2***.

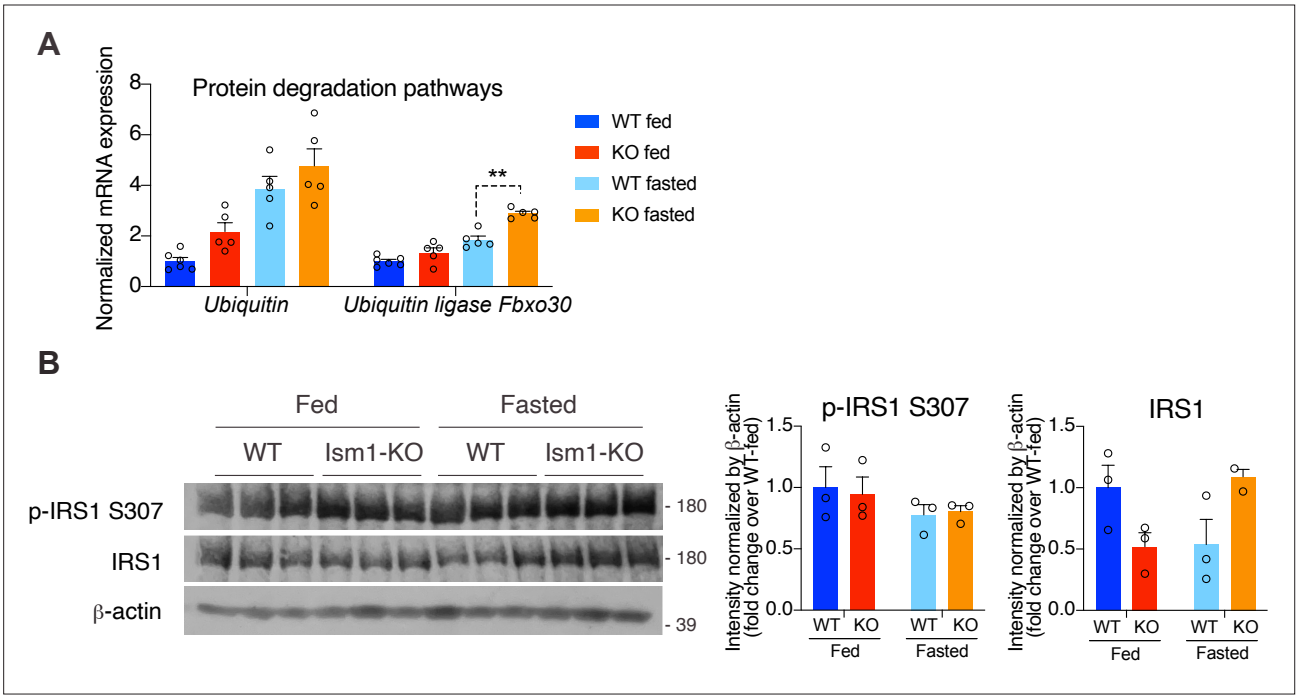

Figure 6—figure supplement 1. Ubiquitin expression and insulin receptor substrate-1 (Irs1/2) phosphorylation status in quadriceps muscles of WT and Ism1-KO mice. (**A**) Relative gene expression analysis of *Ubiquitin* and the ubiquitin ligase *Fbxo30* in quadriceps muscle from WT fed (n = 6) or *Ism1*-KO fed (n = 5) vs. WT fasted (n = 5) or *Ism1*-KO fasted (n = 5) mice. p-Values are calculated by two-way ANOVA, *p<0.05, **p<0.01, ***p<0.001. (**B**) Western blot analysis and quantification of the in vivo levels of p-IRS1 S307, IRS1, and β-actin in quadriceps muscles of WT and *Ism1*-KO mice under fed and fasted conditions (WT fed, n = 3, *Ism1*-KO fed, n = 3, WT fasted, n = 3, *Ism1*-KO fasted, n = 3, two-way ANOVA, *p<0.05, **p<0.01, ***p<0.001). Bar graphs show mean ± SEM.